Electronic Relaxation Dynamics in Coupled Metal Nanoparticles

Mark J. Feldstein,[†] **Christine D. Keating,**[‡] **Yish-Hann Liau,**[†,§]
Michael J. Natan,[‡] **and Norbert F. Scherer*,**[†,§]

Contribution from the Department of Chemistry and Laboratory for Research on the Structure of Matter, University of Pennsylvania, Philadelphia, Pennsylvania 19104-6323, and Department of Chemistry, 152 Davey Laboratory, The Pennsylvania State University, University Park, Pennsylvania 16802-6300

Abstract: This paper reports the results of hot-electron lifetime measurements in a series of thin films prepared by wet chemistry techniques from 12-nm colloidal Au nanoparticles. The films, which vary in thickness and domain (or aggregate) size, are studied by a combined approach of femtosecond optical spectroscopy and scanning probe microscopy. Atomic force microscope measurements are used to characterize the samples and quantify the film's growth pattern. Time-resolved laser spectroscopy measurements are used to determine hot-electron lifetimes. The dependence of the hot-electron lifetimes on the colloid film's structure is analyzed; the lifetimes range from 1 to 3 ps and decrease with greater aggregation. The lifetime is shown to vary in a predictable manner with the film's growth, and a model is presented to describe this relationship. This model allows for the prediction of hot-electron lifetimes over a broad range of film thicknesses and obtains asymptotic agreement with previous experimental results for Au polycrystalline films. Additionally, physical insight into the processes responsible for the range of lifetimes is obtained through an analysis that takes into account two competing phenomena: electron inelastic surface scattering (ISS), which tends to increase electron−phonon coupling with decreasing domain size, and electron oscillation−phonon resonance detuning (EOPRD), which tends to decrease it. The relative contributions of each of these processes has been estimated and shown to agree with the theoretically-predicted tends. Finally, these results have implications for the nature of interparticle coupling and electron mobility. Specifically, they are consistent with and can be taken as evidence for an intercolloid electron conduction mechanism based on activated hopping. In short, the data presented herein and their analysis in terms of a size-dependent ISS and EOPRD shows that in thin films Au colloids aggregate in such a way as to be electronically coupled with one another while being physically separated by organic insulating groups. The films do, however, maintain physical characteristics and electronic influence based on the colloids from which they are built.

Introduction

The development of nanostructured materials is an active area of cross-disciplinary research.[1−5] Promising applications of these materials, especially those based upon organized assemblies of nanoscale colloidal metal particles, take advantage of their unique optical properties. For example, 2-D arrays of noble metal colloids have shown enhancement factors of 10^4 when used as substrates for surface-enhanced Raman spectroscopy.[6] Additional applications of materials built from metal colloids might be based upon the ultrafast response to optical excitation. For example, they have promise as optical switches and as sources of hot electrons for photoelectrochemical processes, including solar energy conversion or organic waste

reduction.[7,8] For applications such as these, it would be ideal to be able to tune, in a controlled manner, the optical response and excitation lifetime. This would be especially important in the case of hot electron transfer to an electron acceptor where, in order to be effective, the electron cooling process should be slower than the time scale required for trapping and relaxation by the electron acceptor.[9,10]

Ultrafast, nonlinear optical measurements on isolated metal colloids both in solution and embedded in a matrix have been previously studied. For example, Heilweil and Hochstrasser have measured the third-order nonlinear susceptibility of aqueous colloidal Au particles at the plasmon resonance and determined optical dephasing times on the order of 20 fs.[11] Stella *et al.* have studied the effect of size on the electronic population dynamics in Sn nanoparticles.[12] They fit the decay of the optically-induced bleach to a series of exponentials with time constants reflecting dynamics on the femtosecond to nanosecond time scales; surface effects were shown to be responsible for

* Author to whom correspondence should be directed.
† University of Pennsylvania.
‡ The Pennsylvania State University.
§ Present address: Department of Chemistry, The University of Chicago, Chicago, IL 60637.
⊗ Abstract published in *Advance ACS Abstracts,* April 15, 1997.

(1) Alivisatos, A. P. *Science* **1996,** *271,* 933.
(2) Harfenist, S. A.; Wang, Z. L.; Alvarez, M. M.; Vezmar, I.; Whetten, R. L. *J. Phys. Chem.* **1996,** *100* (33), 13905.
(3) Mirkin, C. A.; Letsinger, R. L.; Mucic, R. C.; Storhoff, J. J. *Nature* **1996,** *382,* 607.
(4) Alivisatos, A. P.; Johnson, K. P.; Peng, X.; Wilson, T. E.; Loweth, C. J.; Bruchez, M. P., Jr.; Schultz, P. G. *Nature* **1996,** *382,* 609.
(5) Andres, R. P.; Bielfeld, J. D.; Henderson, J. I.; Janes, D. B.; Kolagunta, V. R.; Kubiak, C. P.; Mahoney, W. J.; Osifchin, R. G. *Science* **1996,** *273,* 1690.
(6) Grabar, K. C.; Freeman, R. G.; Hommer, M. B.; Natan, M. J. *Anal. Chem.* **1995,** *67,* 735.

(7) Puech, K.; Blau, W.; Grund, A.; Cardenas, G. *Opt. Lett.* **1995,** *20* (15), 1613.
(8) Hagfeldt, A.; Grätzel, M. *Chem. Rev.* **1995,** *95,* 49.
(9) Lanzafame, J. M.; Palese, S.; Wang, D.; Miller, R. J. D.; Meunter, A. A. *J. Phys. Chem.* **1994,** *98* (43), 11020.
(10) Cavanagh, R. R.; King, D. S.; Stephenson, J. C.; Heinz, T. F. *J. Phys. Chem.* **1993,** *97* (4), 786.
(11) Heilweil, E. J.; Hochstrasser, R. M. *J. Phys. Chem.* **1985,** *82* (11), 4762.
(12) Stella, A.; Nisoli, M.; De Silverstri, S.; Svelto, O.; Lanzani, G.; Cheyssac, P.; Kofman, R. *Phys. Rev. B* **1996,** *53* (23), 15497.

the experimentally measured size dependent lifetimes. Faulhaber *et al.* also measured electronic population dynamics in Au nanoparticles and found a decay time of 7 ps, which is slower than that observed in thin Au films.[13] They attribute this difference to weak electron−phonon coupling and reduced hot-electron transport in the colloids.

This paper reports on the measurement of hot-electron lifetimes in a series of thin films prepared by wet chemistry techniques from 12-nm colloidal Au nanoparticles. These films, which vary in thickness and domain size, are studied by a combined approach of femtosecond optical spectroscopy and scanning probe microscopy. Atomic force microscope measurements are used to characterize the samples and quantify the film's growth pattern, while pump-probe (degenerate four-wave mixing; DFWM) measurements establish the electron thermalization times by detecting the evolution of the collective (*i.e.*, multiple-particle) plasmon resonance. Electron relaxation processes in metals are reviewed in the Theory and Background section. The issue of electron−phonon coupling is addressed along with an overview of experimental and theoretical work that takes into account size effects. The synthetic procedure for the preparation of the colloidal films is outlined in the Experimental Section along with specifics related to the scanning probe and time-resolved measurements. The experimental data are presented in Results and Discussion, and a simple model is used to understand the correlation of hot-electron lifetimes with film structure. The results are further analyzed to extract the relative influence of two competing phenomenon: inelastic surface scattering (ISS), which tends to increase the electron−phonon coupling with decreasing size, and electron oscillation−phonon resonance detuning (EOPRD), which tends to decrease it. The results are shown to be consistent with "activated hopping" as the bulk electron conduction mechanism. Finally, in Summary and Conclusion, an overview of the work is presented and its relevance to the design of optoelectronic devices with synthetically tunable hot-carrier lifetimes is addressed.

Theory and Background

The process causing relaxation of hot electrons in metals has been studied, both experimentally[14] and theoretically.[15] Electrons that are optically excited to energy states of the metal above the Fermi level relax initially by electron−electron (e−e) scattering to states near the Fermi level. In so doing, electrons establish an equilibrium distribution characterized by an electron temperature that is "hot" (*i.e.*, not in equilibrium) relative to the lattice. The model for hot electron relaxation is based on energy transfer via inelastic electron−phonon (e−ph) collisions and thermal diffusion according to the coupled nonlinear differential equations:[14,15]

$$C_e(T_e)\frac{\partial T_e}{\partial t} = K\nabla^2 T - G(T_e - T_l) + A(r,t) \qquad (1a)$$

$$C_l\frac{\partial T_l}{\partial t} = G(T_e - T_l) \qquad (1b)$$

where C is the heat capacity of the metal, K is the thermal conductivity, T is the electron or lattice temperature, G is the electron−phonon coupling constant, $A(r,t)$ represents the spatial and temporal profile of the heating source, and the subscripts "e" and "l" refer to the electron and lattice, respectively. These equations can be simplified by neglecting the following: (i) the slow thermal conductivity term; (ii)

in the case of a femtosecond excitation pulse, the heating source term; and (iii) in the low-fluence, small thermal perturbation limit, the temperature dependence of C_e. Then, after integration, the electron−lattice temperature difference can be written in an alternate form:

$$T_e(t) - T_l(t) = [T_e(0) - T_l(0)]\exp^{-t/\tau} \qquad (2a)$$

where the hot electron lifetime, τ, has the form:

$$\tau = \left(\frac{G}{C_e} + \frac{G}{C_l}\right)^{-1} \qquad (2b)$$

and the initial temperatures of the electrons and the lattice immediately following the excitation pulse are given by $T_e(0)$ and $T_l(0)$, respectively. The temporal dependence of the temperature difference, $T_e(t) - T_l(t)$, can be related to experimentally measured transient reflectivity or, as shown below, transmission signals. Under the condition of $C_e \ll C_l$, as is the case with Au, or in the low-fluence, small thermal perturbation limit where $\partial T_l/\partial t$ can be approximated as zero, further simplification can take place,[16] in particular

$$\tau = C_e/G \qquad (3)$$

with

$$G = \frac{9}{16}\frac{n\kappa_B^2 T_D^2 \nu_F}{16\,\Lambda(T_l)T_l E_F} \qquad (4a)$$

Or, equivalently,

$$G = k_G \nu_{e-ph} \qquad (4b)$$

where the effective electron−phonon collision frequency, ν_{e-ph}, has the form,

$$\nu_{e-ph} = \frac{\nu_F}{\Lambda(T_l)} \qquad (4c)$$

The terms in eq 4 are defined as follows: n is the electron number density, k_B is Boltzmann's constant, T_D is the Debye temperature, ν_F is the electron velocity (Fermi velocity), Λ is the effective electron mean free path, T_l is the lattice temperature, E_F is the Fermi energy, and k_G contains all the terms of G except those accounted for in ν_{e-ph}. As above, by assuming the low-fluence, small thermal perturbation limit, the temperature dependence of the electron mean free path, Λ, can be neglected. This model allows one to directly extract the e−ph coupling term, G, from the experimentally measured decay times by the relation in eq 3. Further, as will be shown below, the effective collision frequency, ν_{e-ph}, can be used as a single parameter to measure or quantify the complicated and competing effects that are relevant to electron dynamics in colloidal metal films of various thickness and aggregation.

These relationships were developed to describe e−ph relaxation in bulk materials. Thus, it is reasonable to expect that, for the limiting case of small colloids or domains (of electrical conduction), size effects will need to be considered. Further, as colloid or small domain films grow from relatively isolated units toward a bulk-like thin film, their physical properties, such as electron−phonon coupling, should undergo a transition between these two limits. For example, the effect of size on electron−phonon coupling has been explored for the case of semiconductor nanocrystals.[17] It has been shown that the coupling of electrons to the longitudinal optical (LO) phonon modes is greatly reduced as the colloid size (*i.e.*, diameter) becomes smaller. The particle size comes into play due to its effect on the increasing overlap of the exciton's electron and hole wave functions as they are confined to ever smaller volumes, thus diminishing the polarity of the excitation. The exciton's polarity is necessary for effective coupling to the LO phonon

(13) Faulhaber, A. E.; Smith, B. A.; Andersen, J. K.; Zhang, J. Z. *Mol. Cryst. Liq. Cryst.* **1996**, *283*, 25.
(14) Fujimoto, J. G.; Liu, J. M.; Ippen, E. P.; Bloembergen, N. *Phys. Rev. Lett.* **1984**, *53* (19), 1837.
(15) Kaganov, M. I.; Lifshitz, I. M.; Tanatarov, L. V. *Soviet Phys. JETP* **1957**, *4*, 173.

(16) Qui, T. Q.; Tien, C. L. *J. Heat Transfer* **1993**, *115*, 842.
(17) Alivisatos, A. P.; Harris, T. D.; Carroll, P. J.; Steigerwald, M. L.; Brus, L. E. *J. Phys. Chem.* **1989**, *90* (7), 3463.

modes.[18] A competing mechanism, the coupling of electrons to acoustic phonon modes, is believed to increase with decreasing colloid size since the structural deformations that occur upon electronic excitation are distributed over relatively fewer modes in nanocrystals as compared to many modes in bulk crystals. Therefore, the coupling of the exciton to each vibrational mode could be stronger.[19]

The physics of semiconductor nanocrystals is, however, different from that of metal colloids since the optical excitation in the former results in the creation of an exciton, not a plasmon as in a metal, and also because these size-dependent e−ph coupling effects have been examined in particles exhibiting quantum confinement of the excitation. Despite these significant differences, it has been found that hot-electron lifetimes in metals are also affected by the domain size of the system.[20−27] In fact, as reported herein, for metallic domains on the order of tens of nanometers in size, two competing phenomena influence the hot electron lifetimes.

Experimentally, hot-electron lifetimes and electron−phonon coupling has been studied in Au systems across a range of domain sizes. Toward the small domain limit (but before quantum size effects would need to be included)[20] are the measurements of El-Sayed *et al.*,[21] where the decay time for a dilute aqueous solution of 15-nm Au colloids was found to be 2.5 ps. This value, which is consistent with previous work,[11] suggests a relatively small coupling constant, with a value of $G = 0.8 \times 10^{16}$ W/(m^3 K).[28] Similarly, Faulhaber *et al.* attributed the relatively slow decay time of 7 ps for 14-nm Au nanoparticles to weak electron−phonon coupling and reduced hot-electron transport.[13] Toward the large domain limit is the work of ElSayed-Ali *et al.* on 20- and 80-nm mono- and polycrystalline Au films.[22] Their results, extrapolated to low optical fluence in order to compare with the present work, predict a decay time of ∼1.2 ps for an 80-nm polycrystalline Au film. As compared to the isolated colloid, their result suggests an e−ph coupling constant that is two times larger.[29] Measurements and predictions of "bulk" Au suggest an electron−phonon thermalization time constant with values in the range of 0.7 to 0.8 ps, indicating a G of 2.67×10^{16} W/(m^3 K).[23] Finally, Brorson *et al.* examined a series of single crystalline Au films ranging from 20 to 200 nm in thickness and observed hot-electron decay times that changed from ∼1.7 to 0.7 ps with increasing thickness.[24] Thus, it appears that in many instances e−ph coupling in metals increases with increasing domain size. This general trend is further supported by the data in the current work.

Theoretically, the reduced electron−phonon coupling responsible for increased hot-electron lifetimes in small metallic domains has been shown to be a consequence of a loss of resonance overlap between the electron-oscillation frequency and the phonon spectral density. Electron-oscillation frequency plasmon resonance detuning (EOPRD) affects the hot-electron lifetimes when the electron oscillation frequency, $\nu_F/2R$ (where R is the domain radius), exceeds the Debye frequency, ω_D, *i.e.*, the upper bound of the phonon spectrum.[25,27] The electron "oscillations" result from reflection of the electron wave function from the boundary of the domain or particle. In this limit, e−ph coupling is significantly reduced due to the lack of resonances overlap required for effective energy exchange. Therefore, in the case of small domains, e−ph coupling results primarily from inelastic electron scattering from the
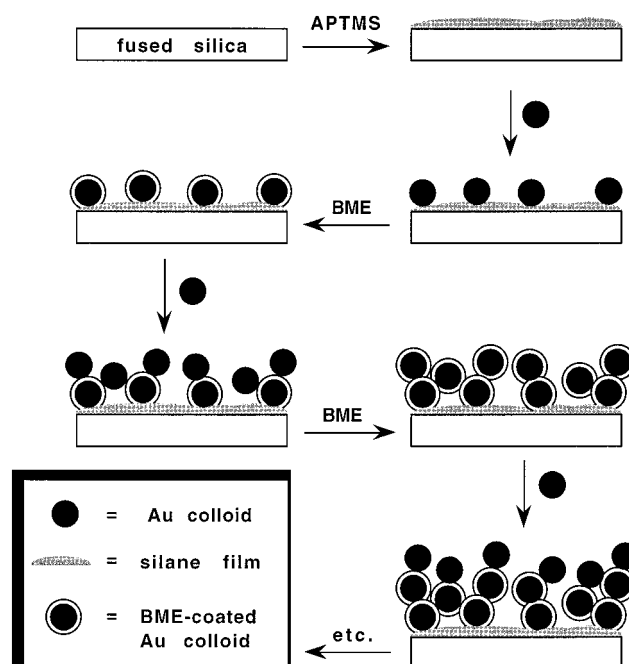
(18) Shiang, J. J.; Risbud, S. H.; Alivisatos, A. P. *J. Chem. Phys.* **1993**, *98* (11), 8432.

(19) Schmitt-Rink, S.; Miller, D. A. B.; Chemla, D. S. *Phys. Rev. B* **1987**, *35*, 8113.

(20) Doremus, R. H. *J. Chem. Phys.* **1964**, *40* (8), 2389.

(21) Ahmadi, T. S.; Longunov, S. L.; El-Sayed, M. A. *J. Phys. Chem.* **1996**, *100* (20), 8053.

(22) ElSayed-Ali, H. E.; Juhasz, T.; Smith, G. O.; Bron, W. E. *Phys. Rev. B* **1991**, *43*, 4488.

(23) Qui, T. Q.; Tien, C. L. *Int. J. Heat Mass Transfer* **1992**, *35*, 719.

(24) Brorson, S. D.; Fujimoto, J. G.; Ippen, E. P. *Phys. Rev. Lett.* **1987**, *59* (17), 1962.

(25) Gorban, S. A.; Nepijko, S. A.; Tomchuk, P. M. *Int. J. Electron.* **1991**, *70* (3), 485.

(26) Belotskii, E. D.; Tomchuk, P. M. *Surf. Sci.* **1990**, *239*, 143.

(27) Wang, W. Y.; Riffe, D. M.; Lee, Y-S.; Downer, M. C. *Phys. Rev. B.* **1994**, *50*, 8016.

(28) $C_e = 2.0 \times 10^4$ J/(m^3 K).

(29) The 20-nm Au films in the Elsayed−Ali study have a decay time that is shorter than that of the 80-nm films. This is not consistent with the trend from isolated colloid to bulk material.

Figure 1. Scheme depicting the stepwise assembly of Au colloid multilayer films; see Experimental Section for details. APTMS and BME represent (3-aminopropyl)trimethoxysilane and 2-mercapto-ethanol, respectively.

domain boundary, a collision that is less effective for energy transfer than e−ph scattering in the bulk. This resonance effect, in the case of Au domains in the size range of 10−40 nm, has been predicted to result in a reduction in e−ph coupling of as much as two orders of magnitude as compared to bulk material.[25,27]

However, in addition to this intrinsic size effect, a second effect that is due to inelastic surface scattering (ISS) needs to be considered. Specifically, e−ph coupling can increase with decreasing size since a surface or domain boundary can act as an important additional site for inelastic scattering. For example, the effect of the colloidal radius on the hot-electron lifetime in tin nanoclusters has been shown to correlate with the surface collision frequency.[12] In this case, decreasing colloid radius results in an increased rate of electron−surface collision and a decreased hot-electron lifetime. The influence of the colloid boundary has also been demonstrated by Zhang *et al.*, who found an almost 50% change in the hot-electron lifetime for 18-nm Au colloids with a change of solvent from water to cyclohexane.[30] This dramatic change clearly shows the importance of the domain boundary on electron dynamics. The impact of grain boundaries on hot electron lifetimes has been most clearly demonstrated by ElSayed-Ali. In a comparison of mono- and polycrystalline thin Au films it was found that hot-electron lifetimes are consistently shorter in the polycrystalline films, *i.e.*, in films with grain boundaries where additional e−ph scattering and coupling can occur.[22] These results were further analyzed and described by a model that accounts for the effect of both the domain size and grain boundaries on increasing electron−phonon coupling.[23]

Experimental Section

1. Colloidal Gold Multilayer Film Assembly. The general procedure for preparation of Au colloid multilayer films is shown schematically in Figure 1. First, a clean hydroxyl- or oxide-terminated substrate is reacted with amine-functionalized organosilane, which polymerizes on the substrate surface, yielding a large number of terminal amino groups oriented away from the substrate. Au particles bind to NH$_2$ groups with high affinity, and consequently self-assemble into submonolayer (*i.e.*, non-epitaxial) films upon exposure to aminosilane-modified surfaces. Submonolayer coverages, typically in the range of 15−30%, are a consequence of interparticle repulsions between the

(30) Zhang, J. Z.; Smith, B. A.; Faulhaber, A. E.; Andersen, J. K.; Rosales, T. J. In *Ultrafast Processes in Spectroscopy IX*; Plenum Publishing Corporation: New York, 1996; pp 561−565.

Table 1. Sample Parameters

sample	deposition cycles	O.D. at 800 nm	$\langle Z(x,y)\rangle$ (nm)
III	2	0.158	5.8
IV	3	0.200	12.1
V	4	0.219	28.8
VI	5	0.262	38.5
VII	6	0.282	47.1
bulk	NA	$60/\mu m$	inf

negatively-charged colloidal particles.[6,31] Additional Au can be deposited atop the submonolayer by exposure of the film to a bifunctional cross-linker, in this case HSCH$_2$CH$_2$OH (2-mercapto-ethanol), which binds to the Au particles and allows deposition of a second "layer" of Au particles. This cross-linking-deposition procedure may be repeated many times to increase the film thickness. It should be noted that there is no registry between Au particles in the multilayer, nor are there distinct layers (see Figures 1 and 3).[32]

Colloidal Au solutions were prepared by citrate reduction of HAuCl$_4$ in aqueous solution as previously described in ref 6. All H$_2$O used in the film preparation was 18 MΩ and came from a Barnstead Nanopure H$_2$O purification system. Au particles were imaged by transmission electron microscopy (TEM) for size analysis. The Au colloids used in this work were slightly elliptical with major and minor axes of 12 ± 1.1 and 11.5 ± 1.0 nm, respectively, where the statistics are based on the analysis of 275 random particles. The program "NIH Image" was used for particle size determination from TEM photographs.[33]

Au colloid submonolayers were prepared by using a modification of published protocols.[6,34] Fused silica substrates were cleaned in "piranha bath" (4:1 ratio of concentrated H$_2$SO$_4$ to 30% H$_2$O$_2$) and rinsed with copious amounts of H$_2$O prior to use.[35-38] Samples were then placed in 10% (3-aminopropyl)trimethoxysilane (APTMS, United Chemical Technologies, Inc.) in methanol for derivatization. Silanized substrates were removed after 2.5 h, rinsed in methanol and then in H$_2$O, and immersed in 12-nm Au colloid solutions for 3.5 h. Au colloid submonolayer films were rinsed in H$_2$O.

A series of five different Au colloid multilayer films were prepared by increasing the number of colloid cross-linking-deposition sequences, as summarized in Table 1, by the following procedure (see Figure 1):[32] samples prepared as above were (i) soaked in 4 mM 2-mercapto-toethanol (Sigma) for 8−10 min, followed by extensive rinsing with H$_2$O, (ii) immersed in colloidal Au solution for 1.5 h or more, and (iii) after rinsing, returned to 2-mercaptoethanol for 8−10 min, and the process was then repeated to form samples with additional "layers" of Au colloids. Subsequent to multilayer formation, samples were rinsed with methanol and allowed to dry in air. Optical spectra were acquired on an HP5482A diode array spectrophotometer, see Figure 2.

2. AFM Measurements. The surface structure and growth patterns of the colloidal Au films were examined with an atomic force microscope, AFM (Nanoscope III, Digital Instruments), with silicon tips. All measurements were carried out in "Tapping Mode" in order to avoid damaging the films.[39,40] In this mode, the AFM cantilever is

(31) Grabar, K. C.; Smith, P. C.; Musick, M. D.; Davis, J. A.; Walter, D. G.; Jackson, M. A.; Guthrie, A. P.; Natan, M. J. *J. Am. Chem. Soc.* **1996**, *118*, 1148.

(32) Musick, M. D.; Keating, C. D.; Keefe, M. H.; Natan, M. J. *Chem. Mater.*, in press.

(33) Written by Wayne Rasbad at the U.S. National Institutes of Health and available from the Internet by anonymous FTP from zippy.nimh.nig.gov or on floppy disk from NTIS, 5285 Port Royal Rd., Springfield, VA, 22161, Part No. PB93-504868.

(34) Freeman, R. G.; Grabar, K. C.; Allison, K. J.; Bright, R. M.; Davis, J. A.; Guthrie, A. P.; Hommer, M. B.; Jackson, M. A.; Smith, P. C.; Walter, D. W.; Natan, M. J. *Science* **1995**, *267*, 1629.

(35) **Caution!** Piranha solution is extraordinarily dangerous, reacting explosively with trace quantities of organics. It should be handled in very small quantities and with great care.

(36) Dobbs, D. A.; Bergman, R. G.; Theopold, K. H. *Chem. Eng. News* **1990**, *68* (17).

(37) Matlow, S. L. *Chem. Eng. News* **1990**, *68* (30).

(38) Wnuk, T. *Chem. Eng. News* **1990**, *68* (26).

(39) Putman, C. A. J.; Vanderwerf, K. O.; Degrooth, B. G.; Vanhulst, N. F.; Greve, J. *Appl. Phys. Lett.* **1994**, *64* (18), 2454.

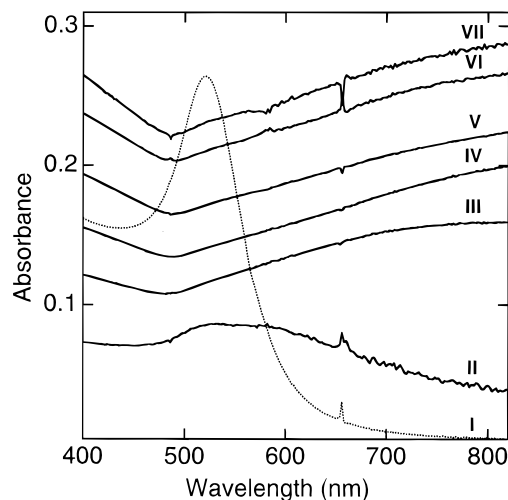(40) Hansma, P. K.; Cleveland, J. P.; Radmacher, M.; *et al. Appl. Phys. Lett.* **1994**, *64* (13), 1738.

Figure 2. Optical spectra for Au colloid multilayers: (I) absorption spectra of 12-nm Au colloids in aqueous solution (∼3.5 nM in Au particles) (the spectrum has been divided by 3 to fit the scale of the graph), (II) single Au deposition film, (III) two Au depositions, (IV) three Au deposition, (V) four Au depositions, (VI) five Au depositions, and (VII) six Au depositions. All spectra except I were taken of dry surfaces in air.

oscillated at its resonance frequency (∼300 kHz) with an amplitude of approximately 20 nm.[41] Multiple images in different areas of each film were taken, and quantitative results reported herein are based on the averages of these measurements.

3. Time-Resolved Measurements. Hot-electron thermalization by e−ph coupling was studied with transient optical transmission measurements, performed with use of a standard pump−probe configuration.[42] The laser system is based on a home-built, cavity-dumped Ti:Sapphire laser. This laser produces sub-20-fs pulses centered at 800 nm with energy in excess of 25 nJ/pulse (peak powers > 10^6 W) with a variable repetition rate, from MHz to sub-kHz. The cavity-dumped pulse is dispersion compensated in a prism-pair sequence and then split into an intense pump and a weak probe pulse. The pump pulse travels along a fixed optical delay line while the weak probe passes through a variable delay line. The two pulses are focused to a common spot on the sample of approximately 75-μm diameter while propagating at near normal incidence. At the sample the pump pulse has an energy of approximately 7.5 nJ, yielding a fluence of ∼0.075 mJ/cm^2, which can be considered to be in the low-fluence regime for the study of metallic systems.[22] The samples were continuously rotated at ∼20 Hz about an axis normal to the surface to provide "fresh" sample and avoid excessively heating a single location.

Results and Discussion

1. Static Optical Properties. In solution, the 12-nm Au colloids used for these samples have an absorption centered at ∼520 nm due to a surface plasmon excitation (see trace I, Figure 2). The close proximity of the colloids in the film results in an additional absorption band not present in the case of isolated colloids. This broad absorption band, red shifted from the single particle plasmon excitation and centered at ∼800 nm, is assigned to a collective particle plasmon excitation and occurs when the interparticle spacing is substantially less than the optical wavelength. The existence of this band is based on electromagnetic coupling between the colloids and has been described by Kreibig.[43,44] Briefly, the plasmon excitation is a dipolar excitation where the conduction electrons oscillate at the optical

(41) Application note: *Tapping Mode Imaging: Applications and Technology*; Digital Instruments: Santa Barbara, CA, 1995.

(42) Arnett, D. C.; Vöhringer, P.; Scherer, N. F. *J. Am. Chem. Soc.* **1995**, *117* (49), 12262.

(43) Quinten, M.; Kreibig, U. *Surf. Sci.* **1986**, *172*, 557.

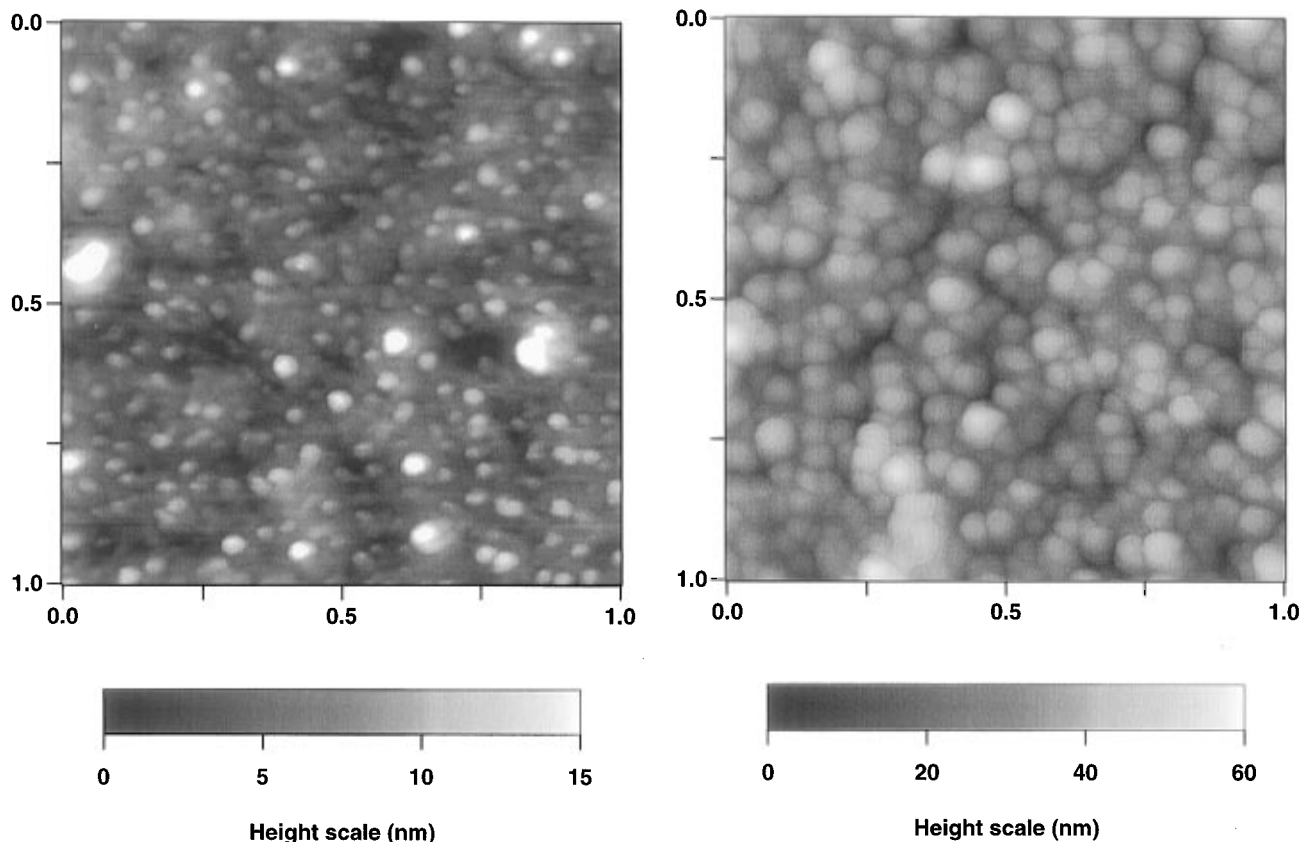(44) Quinten, M.; Schönauer, D.; Kreibig, U. *Z. Phys. D* **1989**, *12*, 521.

Height scale (nm)   **Height scale (nm)**

Figure 3. Tapping mode AFM images of colloidal films III (left) and V (right). The image area in both cases is 1 μm². Film parameters are summarized in Table 1.

frequency between the two extremes of the colloid volume and in the direction of the electric field. When close enough in distance, the electric field of one colloid can couple to and lower the excitation energy of the plasmon in a second colloid. Thus, in a collective plasmon excitation mode the dipoles of the excited colloids are oscillating coherently and with fixed phase relationships. As the colloidal density increases the collective plasmon-band absorption also increases due to increased electronic coupling. The absorption spectra for the films studied here are shown in Figure 2, and their optical densities at 800 nm are summarized in Table 1. The description of the inter-colloid electromagnetic interaction depends in a nontrivial way on both their separation and the detailed geometry in which they are arranged. A number of theoretical approaches have been developed to model and describe the physics of these complex relationships.[45–47] These approaches are based on dipole and higher multipole coupling and have been used to model linear optical responses.

2. Film Growth. The growth of the colloidal films has been studied and quantified by AFM techniques. Images of two of the films are shown in Figure 3. Tip convolution and other effects that blur particle edges are evident in these images.[48] However, it is clear, even from a casual inspection of these images, that there has been vertical growth in the latter film. This height change is evident in the increased range of the Z-axis for the multilayer film. Moreover, lateral growth due to the aggregation of colloids is also apparent.[49] As shown in Figure 4, the growth rate of these films is quantified by the correlation
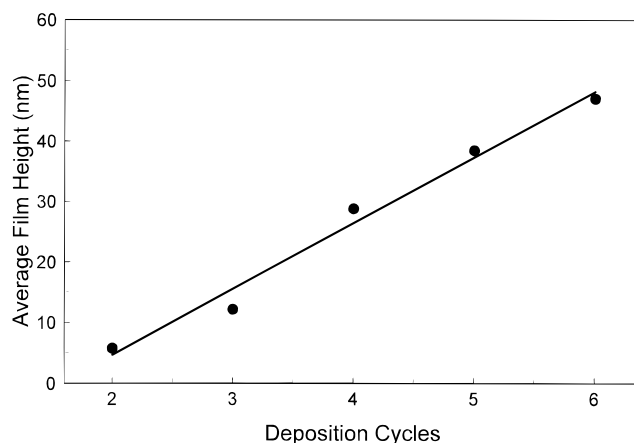

Figure 4. Colloidal film growth pattern. The growth rate is represented by the AFM measured height as a function of the number of deposition sequences, points. A linear fit of these data, solid line, yields the following correlations: $\langle H \rangle = -17.12$ nm $+ (10.89$ (nm/dep) $\times$ *deps*, where $\langle H \rangle$ is the average film height and *deps* is the number of deposition sequences.

between the number of repetitions of the colloid deposition sequence and the average height of the film.[50] These values are listed in Table 1. It can be seen that multiple colloid deposition steps result in film growth that, beginning with the second deposition sequence, is linear in average height. Independent AFM and atomic absorption measurements confirm this growth pattern.[32,51]

(45) Yang, W-H.; Schatz, G. C.; Van Duyne, R. P. *J. Phys. Chem.* **1995**, *103* (3), 869.

(46) Bosi, G. *J. Opt. Soc. Am. B* **1996**, *13* (8), 1691.

(47) Singer, R. R.; Leitner, A.; Aussenegg, F. R. *J. Opt. Soc. Am. B* **1995**, *12* (2), 220.

(48) Grabar, K. C.; Brown, K. R.; Keating, C. D.; Stranick, S. J.; Tang, S-L.; Natan, M. J. *Anal. Chem.* **1997**, *69*, 471.

(49) Presumably, as depicted in Figure 1, previously deposited colloids act as nucleation sites for additional growth and, hence, colloidal aggregates are formed.

(50) There is a limit on the range of height measurements of these films with an AFM. These measurements can only be accurate while the film is still discontinuous so that a reference point of zero height exists.
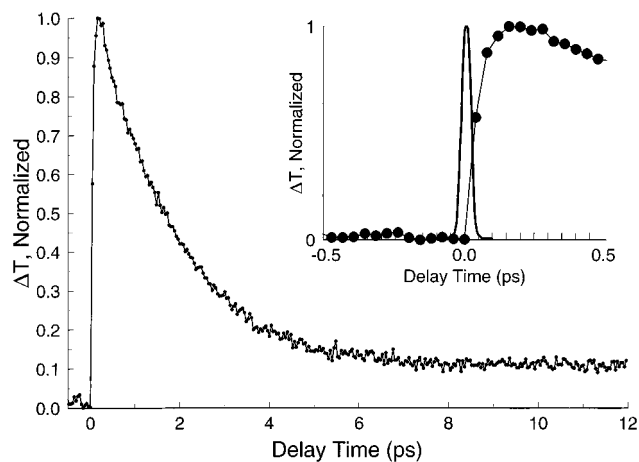
Electronic Relaxation Dynamics in Coupled Metal Nanoparticles

J. Am. Chem. Soc., Vol. 119, No. 28, 1997 6643

Figure 5. Time-dependent 800-nm pump-probe response of colloidal Au film III (points with solid line). ΔT is the pump-induced change in the wavelength-integrated probe transmission through the sample. The inset shows early time dynamics (points with solid line) and the laser autocorrelation function (solid line).

Figure 6. Pump-probe data in semilog format for colloidal Au films III (▲), IV (▼), V (■), VI (◆), and VII (●). Exponential fits, beginning at 240 fs, of the form described in eq 5 are shown as solid lines. Parameters from data analysis are summarized in Table 2.

An understanding of the growth process is important for understanding the physical and electronic properties of the resultant film. Inspection of the AFM images suggests that this growth is due to the aggregation of the colloids. One can differentiate between aggregation and coalescence, the former being the bunching together of particles close to each other, up to the point of contact. The latter implies growth by the "fusion" of adjacent particles to form a single larger domain. Clearly, growth by coalescence eventually results in formation of a bulk film with uniform physical and electronic properties. It is believed that the growth of the present films occurs by aggregation since (i) the colloid surfaces are coated and effectively passivated with 2-mercaptoethanol and (ii) the AFM images reveal gaps between the colloids. Further, it has been shown that the DC resistance of the colloidal multilayers is dependent on the alkyl chain length of the organic cross-linker.[32] Thus, the organic layer does "insulate" the colloids and prevent metal−metal contact. It is nevertheless apparent that the colloids are grouped together in such a way as to be coupled both spatially and electronically. Spatial coupling, as noted previously, is relevant to the effective electrically coupled domain size(s) in the film. Coupling within the growing domains is indicated by the decay time of the signal associated with hot-electron thermalization by electron−phonon scattering. This coupling is relevant to electrical conduction in the colloidal films. Electronic (*i.e.*, dipolar) coupling is apparent in the changes in the absorption spectra, as noted above in Figure 2, where the collective plasmon band forms as the colloid deposition proceeds.

3. Hot-Electron Lifetimes. A representative pump-probe response for the 3-layer film is shown in Figure 5 along with the pulse cross correlation function. This time-resolved DFWM signal results from a transient bleach at the multiparticle plasmon resonance frequency due to the generation of a non-equilibrium electron distribution. That is, upon excitation of the collective plasmon, some electrons are highly excited. The collective plasmon rapidly (*i.e.*, *circa* 10 fs) dephases such that the

collective electronic excitation becomes an incoherent population of hot electrons.[11,52] The subsequent relaxation by e−e scattering actually causes more electrons in the system to become non-thermal with respect to the lattice. As a result there is a depletion of the equilibrium electrons that can contribute to subsequent collective plasmon excitation by the probe pulse, hence the probe pulse transmission is transiently enhanced. The pump-pulse perturbation of the colloid film system from equilibrium yields the rise in probe-pulse transmission, while restoration of the system to equilibrium causes the induced signal to go to zero, as if the pump-pulse perturbation never occurred.[53,54]

These electron dynamics are clearly exemplified by the current data. Specifically, the early time response, at <200 fs, shows a rise significantly slower than the excitation pulse duration. These early time dynamics can be attributed to electron thermalization by e−e scattering.[14,15] The rise time for these signals can be approximated with an exponential time constant in the range of 50−100 fs, depending on the mathematical model and analysis method used to fit the data set, and are consistent with previous measurements of this process.[14,15] Choice of an appropriate model to fit the rise is complicated by the fact that the e−e scattering process is energy dependent, which means that a detailed study of e−e scattering requires an energy-resolved analysis. This can be achieved through methods such as energy-resolved electron detection or wavelength-resolved pump-probe measurements.[55,56] Thus, the data presented herein can only capture an integrated e−e scattering response, for which there is no clear model. Consequently, the early time dynamics, which within experimental error are independent of film composition and domain size, are not included in any further analysis of the data.[12]

The normalized pump-probe responses for all five colloidal films are shown in semilog format in Figure 6. An exponential decay is clearly evident for all samples. However, the increased optical density and optical scattering in the case of the most

(51) The average film height was measured and used to quantify the colloidal film's growth and aggregation for a number of reasons. First, as noted, it is a representative and characteristic measure of the growth process and is consistent with other measures. Second, as discussed below, the growth in height is correlated to the measured intra- and inter-colloid dynamics. Finally, growth measured in terms of average film height allows for direct extrapolation to and comparison with the bulk, polycrystalline limit.
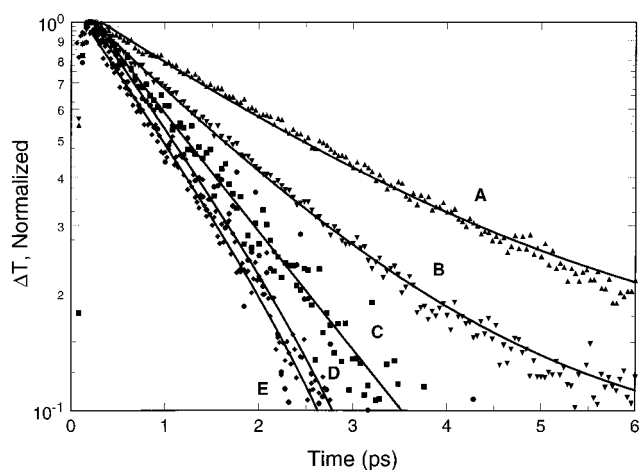
(52) Yang, T. S.; Vöhringer, P.; Arnett, D. C.; Scherer, N. F. *J. Chem. Phys.* **1995**, *103* (19), 8346.

(53) Chandler, D. *Introduction to Modern Statistical Mechanics*; Oxford University Press: New York, 1987; Chapters 4 and 8.

(54) Mukamel, S. *Principles of Nonlinear Optical Spectroscopy*; Oxford University Press: New York, 1995; Chapter 17.

(55) Fann, W. S.; Storz, R.; Tom, H. W. K.; Borkor, J. *Phys. Rev. B* **1992**, *46*, 13592.

(56) Bigot, J. Y.; Merle, J. C.; Cregut, O.; Daunois, A. *Phys. Rev. Lett.* **1995**, *75* (25), 4702.

Table 2. Measured Lifetime and Model Analysis Parameters

sample	τ (ps)	offset, a	G (W/(m³ K))/ 10^{16}	ν_{e-ph} (ps⁻¹)	ISS	EOPRD
III	2.48	0.126	0.807	12.4	5.75	11.91
IV	1.73	0.080	1.16	17.5	4.03	5.82
V	1.40	0.004	1.43	22.3	3.13	3.66
VI	1.31	−0.047	1.53	23.5	2.96	3.23
VII	1.28	−0.049	1.57	24.1	2.87	3.06
bulk	∼0.7	NA	2.67	35.6	1	1

dense samples results in a diminished signal-to-noise ratio (SNR). The exponential decays were fit, using a nonlinear least-squares (NLS) routine, by the following function:

$$S = a + b\exp\left(\frac{-t}{\tau}\right) \quad (5)$$

Because of the fast e−e scattering process the waveforms were fit beginning at 240 fs.[57] The offset, a, was included to account for any slow equilibration process, such as thermal conduction (K, in eq 1), and is responsible for the slight curvature in the tails of the fits. For the two slowest decays, films A and B, the constant term was 12.6 and 8.0% of the peak value, respectively. The offset is an order of magnitude smaller for the next fastest decay, film C. These results suggest that slow thermal processes become important for systems where the e−ph decay is in the range of ∼2 ps or greater. Slow thermal processes have been previously reported in other Au colloid systems.[58] For the two fastest decays, films D and E, the constant terms are small and negative. These offsets are probably an artifact resulting from the lower SNR in these signals. The amplitude factor, b, is near unity for all films since each waveform is normalized to a maximum of 1. As explained below, the decay constant, τ, is the most meaningful result of this analysis. These values and their corresponding offsets, a, are summarized in Table 2.

4. Correlation of Hot-Electron Lifetimes with Film Structure. The electron relaxation dynamics in the series of Au colloidal films are clearly affected by the film's structure. The hot-electron lifetime decreases from a value of 2.5 ps to 1.3 ps as the number of deposition cycles increases and the Au films grow more optically dense. Following the model for electron thermalization via e−ph coupling described in section II and using eq 3, one can directly calculate the value of the e−ph coupling constant, G, for each film. These values are listed in Table 2. The coupling described by G in eq 3 is not constant between the different films. Since the AFM measurements have shown that the spatial dimensions of the films differ, it would be reasonable to conclude that the parameter responsible for the variation of G is also a spatial function. From an examination of the form of G, as detailed in eq 3, the effective electron mean free path, Λ, is the one parameter that relates to the spatial properties of the system. Further, Λ has been shown previously in other systems to account for variable e−ph coupling constants.[23] One can assume, based on the phenomenological result of increasing e−ph coupling with increasing film growth, that Λ has the form:

(57) The analyzed time constants obtained with use of an exponential rise and exponential decay plus offset model were similar. However, as per the preceding discussion about the appropriate functional form for the time dependence of e−e scattering, it was felt that a more reliable analysis was to fit the decay function beginning after the e−e thermalization process is complete.

(58) Pener, M.; Bost, P.; Pauck, T.; von Plessn, G.; Feldmann, J.; Brecker, U.; Menning, M.; Porstendorfer, J.; Schmitt, M.; Schmidt, H. In *Ultrafast Phenomena X*; Barbara, P. F., Fujimoto, J. G., Knox, W. H., Zinth, W., Eds.; Springer-Verlag: Berlin, 1996; pp 437−438.
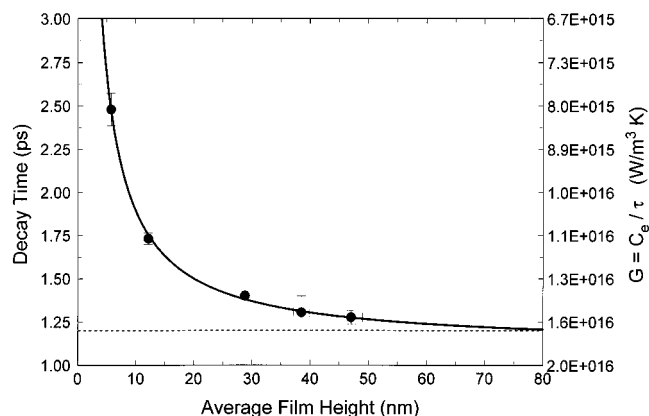

Figure 7. Experimentally determined time constant, τ, and e−ph coupling constant, G, shown as a function of AFM measured average film height, points. Vertical and horizontal error bars indicated standard deviation of the time constant's exponential fit and averaged film height, respectively. The solid line is a NLS fit of the time constant data by eq 3, with Λ from eq 6 using the average height data for SP, the surface property. The dashed horizontal reference line marks the time constant for 80-nm polycrystalline Au film, extrapolated to a low and comparable optical excitation fluence.[22]

$$\Lambda = \Lambda_B + \frac{K}{SP} \quad (6)$$

where Λ_B is the effective electron mean free path in the bulk limit, K is a proportionality constant, and SP is an empirically determined spatial property of the film, such as average height. This form gives the correct empirical trend, *i.e.*, as the film grows Λ and G both approach their bulk values. The spatial property, SP, of the film can be directly measured with scanning probe techniques as noted above; the values of the average film height are listed in Table 1. Quantitatively, a NLS fit of the time constant data by eq 3 with Λ from eq 6 yields an exceptionally good fit as a function of the average height, as shown in Figure 7. The value determined for Λ_B is 50.4 nm; this can be compared with the value of 39 nm derived from resistivity measurements of bulk Au.[23]

The relationship between decay time and film growth can be interpreted as showing that the electron−phonon coupling increases through the process of colloidal aggregation and the formation of larger domains due to inter-colloid interactions. As the colloidal films become more aggregated and more optically dense (hence evolving toward the limit of an extended film) the coupling constant, G, asymptotically approaches that of bulk polycrystalline Au. In fact, extrapolation of the fit shown in Figure 7 shows that as the film approaches a thickness of 80 nm the predicted value of the time constant matches the experimental result of ElSayed-Ali for 80-nm polycrystalline film,[22] when the latter is extrapolated to a low and comparable optical excitation fluence. This correspondence further supports the model used herein as being both accurately descriptive of the data and useful as a prescription for the design of devices with synthetically tunable hot-carrier lifetimes.

It should be re-emphasized that Λ represents an *effective* mean free path. That is, Λ is not the distance an electron can travel before a collision (this distance would be a maximum of 12 nm for the Au colloids) but the distance between inelastic collisions that result in energy transfer to the lattice. The trend of increasing Λ with decreasing domain size can perhaps be better understood when examined from the perspective of the effective collision frequency, ν_{e-ph}. This parameter, which describes the frequency of significant inelastic electron−phonon collisions, is readily determined from the knowledge of Λ and with the relation in eq 4c. The values of ν_{e-ph} calculated for

each film are listed in Table 2. The number and frequency of effective collisions are increased in the thicker films with larger domains. Equivalently, the overall frequency of inelastic electron−phonon collisions is reduced in the smaller domain systems even though the total surface collision frequency for 12-nm colloids is quite large, on the order of 10^3 ps^{-1}.

As outlined previously, reducing the domain size shifts the electron oscillation frequency above that of the phonons and e−ph coupling, or, equivalently, ν_{e-ph} is significantly diminished. The reduction in coupling due to EOPRD is predicted to be on the order of 100 while reductions in the range of ten are observed.[25,27] However, as the domain size decreases the electrons will encounter the boundaries more often. Thus, as was the case with Stella,[12] decreasing colloid size would be predicted to result in increased e−ph coupling simply by virtue of the increased surface collision rate and the resultant increase in ISS. In order to account for the results presented here it appears that both of the two competing effects, EOPRD and ISS, factor into the hot-electron lifetime and e−ph coupling measured for the colloidal Au films.

These two effects can be combined by assuming the following simple form for the net effect on coupling:

$$\frac{G}{G_B} = \frac{\nu_{e-ph}}{\nu_{e-ph(BULK)}} = \frac{ISS}{EOPRD} \qquad (7)$$

The ratio G/G_B ($=\nu_{e-ph}/\nu_{e-ph(BULK)}$) represents the relative enhancement (or reduction if the value is less than 1) of the measured coupling, G (or collision frequency, ν_{e-ph}), as compared to the value in the bulk limit, G_B (or $\nu_{e-ph(BULK)}$). This ratio is plotted as a function of film thickness in Figure 8a. The enhancement factor, ISS, results from the existence of the proximal colloid surface as an additional source for e−ph coupling and the reduction factor, EOPRD, takes into account the detuning of resonance overlap between the electron oscillation frequency and the phonon spectrum.

The value of ISS can be estimated from the model outlined by Qui and Tien and previously applied to thin polycrystalline Au films, which takes into account both the domain size and the film thickness:[23]

$$ISS = 1 + \frac{3}{8\beta}(1 - P) + \frac{7}{5}\alpha \qquad (8)$$

where β is a film thickness parameter defined as d/Λ and d is taken as the average film height, P is a specular reflection parameter of the electron from the film surfaces and is taken to be zero, α is the grain diameter parameter defined as $(R/1 - R)(\Lambda/D)$, where D is the grain size and is fixed at 12 nm for the colloids presently under study, and R is the reflectivity of electrons at grain boundaries and is taken to be ~0.2.[59] The values of ISS for each film, listed in Table 2 and shown graphically for a continuous range of film thickness in Figure 8a, have the expected trend of increasing with decreasing film dimension as collisions with the boundary become more frequent.

The value of EOPRD can now be solved for by using eq 7; these values are listed in Table 2 and shown in Figure 8a. Again, the trend anticipated in the work of Tomchuk[25,27] is found: EOPRD increases with decreasing dimensions as the electron-oscillation frequency goes farther out of resonance with the upper limit of the phonon spectrum. The calculated EOPRD for the smallest film begins to approach yet never reaches the two orders of magnitude predicted by Tomchuk for nanometer scale metal islands. This is not surprising since the reflectivity

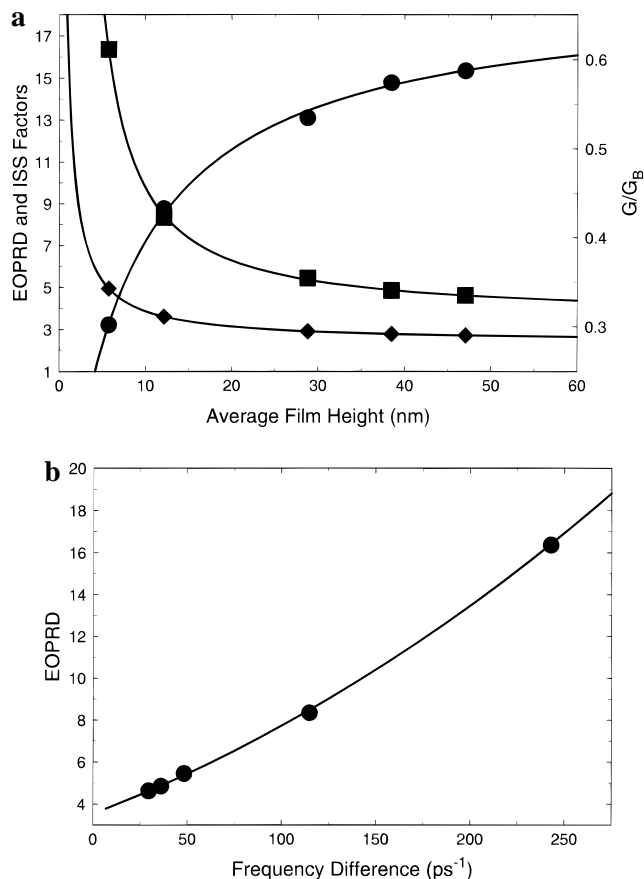(59) de Vries, J. W. C. *Thin Solid Films* **1988**, *167*, 25.

Figure 8. ISS and EOPRD enhancement and reduction factors of the e−ph coupling constant, G. (a) Shown as function of average film height are the ratio of G to the bulk value, G_B, (●), with the solid line based on the functional form of G vs height from the NLS fit shown in Figure 7, ISS (■), with the solid line for the continuous height range, calculated from eq 8, and EOPRD (◆), with the solid line for continuous range, determined by the relation in eq 7. (b) The reduction factor EOPRD is shown as a function of the electron oscillation−phonon spectrum frequency difference: experimental data points with the solid line based on a continuous height range.[60] Parameter values for each film are summarized in Table 2.

factor, R, used to calculate ISS in eq 8, may not appropriately take into account surface defects and traps or the elliptical boundary conditions relevant to the colloids. These factors could yield a reduced value for R and increased coupling leading to a larger theoretically estimated value for EOPRD. Nevertheless, the fact that *both* trends agree with theoretical predictions makes it possible to conclude that the two phenomena are in competition and that a balance between them yields the effective electron−phonon coupling determined experimentally herein.

An even more significant conclusion from these results is that electrons exhibit inter-colloid mobility even though the colloids are not in direct metallic contact. This must be the case since, as shown in Figure 8b, EOPRD correlates with the electron oscillation−phonon spectrum frequency difference. Here, the domain size used to determine the electron oscillation frequency is the average film thickness (related to the aggregate size), not the single particle radius.[60] Thus, if the EOPRD changes with film growth it can only be the case that the electrons are not confined to the volume of a single colloid but are mobile within the aggregated domains. Electron mobility

(60) The frequency difference is calculated as:

$$(v_F/\langle H \rangle) - \omega_D,$$

where v_F is the electron (Fermi) velocity, $\langle H \rangle$ is the average film height, as determined by AFM, and ω_D is the Debye frequency, $(2.2 \times 10^{13}$ s$^{-1})$.[25]

in this system is also consistent with the fact that electrons exhibit enhanced tunneling probability (vs vacuum) through functionalized alkane chains.[61-65] However, the electron dynamics in colloidal Au films are different than in bulk metals where electrons are fully mobile. Specifically, the apparent non-zero intercept of the curve in Figure 8b suggests that even for films with the greatest aggregation (*i.e.*, smallest frequency difference) the electrons lack compete mobility and the colloidal size still maintains an influence on the e−ph coupling.

This analysis has implications for understanding and defining the effective domain size of the colloidal film. The importance of the domain size for electron dynamics is clear since both of the phenomena, ISS and EOPRD, use the measured film height as a parameter. The fact that for each of the phenomena the experimental and predicted trends agree suggests that this analysis is valid. It may, therefore, be concluded that the electronic properties of the film (and the domains within the film) are, in fact, different from the isolated colloids from which they are built. Further, these results can be interpreted as directly probing the length scales and packing densities required for inter-colloid coupling. The most dramatic change in coupling occurs in the region where the film thickness changes from 10 to 30 nm before beginning to plateau at greater thicknesses. This correlates well with the dramatic decrease in surface resistance measured for similar films and attributed to a percolation threshold[66] where a domain has achieved macroscopic dimensions. Specifically, the film's resistance decreases exponentially after the average film thickness reaches approximately 30 nm.[32,67]

The corresponding thresholds of the e−ph coupling constant and electrical resistance suggest that the mechanism responsible for inter-colloid electron mobility, as implied by the dependence of EOPRD on film growth, is directly related to the mechanism responsible for DC conductivity. Specifically, activated hopping between nearest neighbors has been suggested as the mode of electron transfer for colloidal and granular metal films.[32,68,69] This mechanism, where electron transfer between metallic regions is governed by an activation barrier associated with carrier creation and a strong distance dependence due to an exponentially decaying tunneling probability, is consistent with the packing density-dependent e−ph coupling results discussed above. In short, the data presented herein and their analysis in terms of size-dependent ISS and EOPRD phenomena show that in thin films Au colloids aggregate in such a way as to be electronically coupled with one another while being physically separated by organic insulating groups. The films do, however,

maintain physical characteristics, *e.g.*, particle size and surface area, and electronic influence, *e.g.*, inelastic surface scattering, based on the colloids from which they are built.

Summary and Conclusion

Hot-electron lifetimes in an array of synthetically prepared thin films composed of 12-nm colloid Au nanoparticles have been found to vary from 1 to 3 ps in a predictable manner with the film's growth. These responses were measured with femtosecond optical spectroscopy techniques that detect the transient photobleach signal arising from hot-electron relaxation via electron−phonon coupling. Coupling between aggregated particles has been shown to be of significant importance for the optical and electronic properties of the colloidal films. This coupling takes the form of both the well-known dipolar coupling to produce the collective plasmon optical resonance at ∼800 nm and the newly reported inter-colloid coupling that increases the hot-electron decay rate due to inelastic electron−phonon collisions. The mesoscopic structure of the films has been measured with scanning probe microscopy techniques, and a simple model is reported that accounts for the dependence of the hot-electron lifetime on the film's structure. This model also allows for interpolation and extrapolation to predict carrier dynamics across a broad range of colloidal films. Two competing phenomena, inelastic surface scattering, which tends to increase electron−phonon coupling with decreasing domain size, and electron−oscillation phonon resonance overlap detuning, which tends to decrease it, are shown together to determine the hot-carrier lifetimes. The relative contributions of each of these processes has been determined and agree with predicted trends. Finally, the results are shown to be consistent with the DC electrical conductivity mechanism of percolation based on activated hopping.

The implications of this work may be valuable to direct research and development in device applications. For example, the development of practical optoelectronic devices necessitates a working understanding of the relationship between structural features and performance characteristics. This is especially true in the case of nanostructured materials where significant differences exist as compared to bulk material and where these differences may not be readily predictable. For example, the carrier lifetime in an optical switch or gate determines the rate at which the devices can operate. It has been shown here that the structural features of colloidal metal films strongly influence the lifetime of optically pumped electrons and, hence, the potential repetition rate (*i.e.*, bit rate) of a device based on this technology. The results reported herein suggest a guide, one of potential technological importance, for the design of optoelectronic devices with synthetically tunable hot-carrier lifetimes.

Device fabrication could also be advanced by the combination of colloidal metal films with other technologies. This would be especially true when combined with technologies that are both readily prepared and which offer complimentary tunable optical and or electronic properties. For example, the combination of small metal colloids with polymers has already been suggested for the development of nonlinear optical devices with enhanced nonlinear responses.[70] However, the ability demonstrated herein to tune the colloid's optical response and carrier lifetimes by controlling their packing density could have significant practical benefits in terms of optimizing a desired response. Further, it has been found that carrier lifetimes in conducting polymers, such as polyaniline, are also synthetically

(61) Chidsey, C. E. D.; Murray, R. W. *Science* **1986**, *231*, 25.

(62) Stranick, S. J.; Kamna, M. M.; Krom, K. R.; Parikh, A. N.; Allara, D. L.; Weiss, P. S. *J. Vac. Sci. Technol. B* **1994**, *12*, 2004.

(63) Finklea, H. O.; Hanshew, D. D. *J. Am. Chem. Soc.* **1992**, *114*, 3173.

(64) Smalley, J. F.; Feldberg, S. W.; Chidsey, C. E. D.; Linford, M. R.; Newton, M. D.; Liu, Y-P. *J. Phys. Chem.* **1995**, *99*, 13141.

(65) The through-bond electron tunneling rate constant decay parameter has been found to be on the order of 1 per methyl group.[63,64] Given the limiting rate constant, $k_{n=0} = 6 \times 10^8$ s^{-1}, the number of methyl groups in the cross-linker, the number of carriers per colloid as 5×10^4,[55] and assuming a first-order rate equation, one would expect an electron transfer rate on the order of 100 fs. If the number of cross-linkers between adjacent colloids is taken into account, an even higher rate would be predicted. Thus, the rate of electron mobility is significantly faster than the e−ph coupling times reported herein, and it is reasonable to predict that electron dynamics within a given colloid are sensitive to the presence of adjacent colloids.

(66) Cusack, N. E. In *The Physics of Structurally Disordered Matter*; Adam Hilger, and Briston: Philadelphia, 1987; pp 227−65.

(67) Musick, M. D.; Keating, C. D.; Keefe, M. H.; Natan, M. J. Unpublished data.

(68) Adkins, C. J. In *Metal-Insulator Transitions Revisited*; Edwards, P. P., Rao, C. N. R., Eds.; Taylor and Francis: London, 1995; pp 191−210 and references therein.

(69) Mott, Sir N. F. *Conduction in non-crystalline materials*, 2nd ed.; Claredon Press: Oxford, 1993.

(70) Gillberg-LaForce, G. E.; Khanarian, G. *Organic-inorganic composites with enhanced nonlinear optical response.* U.S. Patent 4,913,845, 1990.

tunable.[71] Specifically, carrier lifetimes are increased in polyaniline films as they are made more conductive by secondary doping methods. Thus, in principle, a nonlinear optical or electronic device based on the combination of these technologies would enable greater control over optical response and carrier dynamics and, hence, performance.

(71) Feldstein, M. J.; Zheng, W.; Liau, Y. H.; MacDiarmid, A. G.; Scherer, N. F. Submitted for publication.